

See discussions, stats, and author profiles for this publication at: <https://www.researchgate.net/publication/321811458>

Differential pressure control of 3D printed soft fluidic actuators

Conference Paper · September 2017

DOI: 10.1109/IROS.2017.8206523

CITATIONS

42

READS

2,404

7 authors, including:



Tom Kalisky

University of California, San Diego

4 PUBLICATIONS 50 CITATIONS

[SEE PROFILE](#)



Benjamin Shih

Harvard University

21 PUBLICATIONS 622 CITATIONS

[SEE PROFILE](#)



Dylan Drotman

University of California, San Diego

10 PUBLICATIONS 374 CITATIONS

[SEE PROFILE](#)



Eliah Aronoff-Spencer

46 PUBLICATIONS 2,607 CITATIONS

[SEE PROFILE](#)

Some of the authors of this publication are also working on these related projects:



KidPrint [View project](#)



Apps for Leishmaniasis in rural area in Colombia [View project](#)

Differential Pressure Control of 3D Printed Soft Fluidic Actuators

Tom Kalisky¹, Yueqi Wang¹, Benjamin Shih¹, Dylan Drotman¹, Saurabh Jadhav¹, Eliah Aronoff-Spencer² and Michael T. Tolley¹

Abstract—Fluidically actuated soft robots show a great promise for operation in sensitive and unknown environments due to their intrinsic compliance. However, most previous designs use either flow control systems that are noisy, inefficient, sensitive to leaks, and cannot achieve differential pressure (i.e. can only apply either positive or negative pressures with respect to atmospheric), or closed volume control systems that are not adaptable and prohibitively expensive. In this paper, we present a modular, low cost volume control system for differential pressure control of soft actuators. We use this system to actuate three-chamber 3D printed soft robotic modules. For this design, we find a 54% increase in achievable blocked force, and a significant increase in actuator workspace when using differential pressure actuation as compared to the use of only pressure or vacuum. The increased workspace allowed the robot to achieve complex tasks such as writing on a screen with a laser pointer or manipulating fragile objects. Furthermore, we demonstrate a self-healing capability of the combined system by using vacuum to actuate ruptured modules which were no longer responsive to positive pressure.

I. INTRODUCTION

A. Background

Drawing inspiration from nature, the high compliance of soft robots results in advantageous features including large active and passive continuous deformations, and the ability to absorb energy from impact without damage [1]. These qualities make soft robots favorable over rigid-bodied robots for interaction with humans [2], handling of delicate and fragile objects [3], [4], and for maneuvering in unknown and variable, or sensitive environments [5]–[7]. Based on this promise, recent work has proposed to use soft robotics for medical devices for minimally invasive surgery [8], and diagnosis [9], and safe robotic assisted home care [10].

Despite their advantageous capabilities, and in fact due to the same qualities, general approaches to control and actuation of soft robots are open challenges [1], [11]. The compliant nature of soft robots requires a different control system than a conventional hard-body robot and makes the task of driving such robots challenging. Several methods have been proposed for the actuation of soft robots; one commonly used approach is shape memory wires which deform to a desired shape when heated [12]. Another emerging approach is electroactive polymers which are adopted for actuators and sensors as they change shape and size when

*This work was supported by the Office of Naval Research grant number N000141712062.

¹These authors are with the Department of Mechanical and Aerospace Engineering at the University of California, San Diego (UCSD), 9500 Gilman Dr, La Jolla, CA 92093 USA.

²This author is with the Qualcomm Institute at the University of California, San Diego (UCSD), 9500 Gilman Dr, La Jolla, CA 92093 USA.

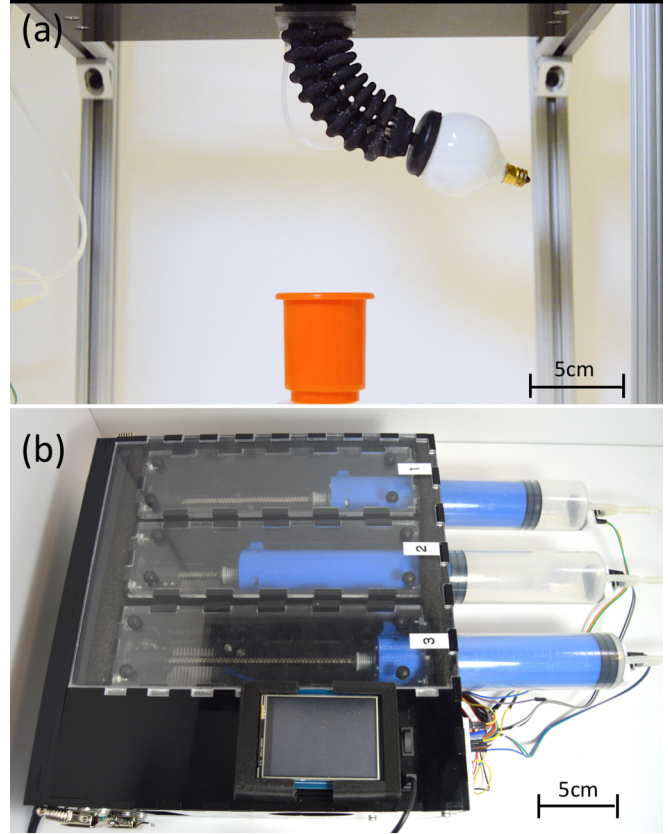


Fig. 1: Closed system for differential pressure actuation and control of 3D printed soft fluidic actuators. a) Demonstration of actuation and manipulation of a delicate object. b) Volumetric control system for positive and negative, pneumatic or hydraulic actuation of soft robotics.

exposed to an electric field, and vice versa [13]. Actuating a soft robot by pulling on properly positioned tensile cables that act like biological tendons is another technique that takes advantage of the high tensile loading capabilities of cables while still being sufficiently compliant to prevent any bending or compression constraints on the soft body [4]. Fluidic Elastomer actuators (FEAs) [11], [14]–[16] take advantage of the ability of a pressurized fluid to adjust itself to apply even pressure on a containing boundary to maintain an adaptive yet consistent mechanism for soft robotics. Most soft robots powered by either pneumatics [14] or hydraulics [17] employ a pump and a system of valves that control internal fluid flow to inflate and deflate their actuators [14]. These open (pump and valves) systems frequently use the pulse-width

modulation (PWM) to switch on the solenoid valves for pressure control. Although very simple and relatively easy to implement, the open systems are noisy and inefficient. Therefore, other methods have been developed which use a closed system control with a cylinder-piston design which allows for a more precise volume regulation while coupling each cylinder with an actuated segment [18], [19]. This coupling eliminates the exhaust of pressurized air to the environment, reducing a key source of energy loss, resulting in increased efficiency and reduced noise. Furthermore, a high gear reduction between motor and piston allows the soft modules to hold position with minimal actuator effort. Although they are very efficient, commercially available syringe pumps are not only expensive but typically designed for small volumes and flow rates [20]. A previously developed volume control systems for soft robots likewise employ expensive components [3]. Furthermore, previous systems have not demonstrated simultaneous pressure and vacuum operation, or the ability to use a variety of working fluids for soft robotics.

B. 3D Printed Soft Actuator

Soft actuators pose many challenges not only in control but also in design and fabrication [21]. Commonly used fabrication techniques for FEA actuators such as soft lithography [22], [23] require many steps and are either limited to the fabrication of 2.5 D structures or require complex 3D molding techniques. To avoid these laborious fabrication processes, we, and other soft roboticists have adapted the use of 3D printers for the task [24]–[27]. The high resolution and the capability of printing multiple materials in a single part enable the facile, rapid fabrication of complex actuator designs. Despite the advantages of 3D printing, challenges in the design of actuators remain due to uncertainty in the materials deposition pattern making the characterization of 3D printed soft actuators very challenging, and the materials themselves are often proprietary or poorly characterized. To test our hypothesis for the functionality of the system and improved performance of 3D printed soft fluidic actuators we used a modular actuator design incorporating three parallel, externally connected chambers rotated 120 degrees about the longitudinal axis of the actuator [14]. In previous work, we proposed a 3D printed bellowed version of this design (Fig. 3) [27]. The actuator was fabricated using a multi-material 3D printer (Objet 350 Connex 3, Stratasys) printed from a rubber-like material (FLX9070-DM), a mixture of a rigid (VeroClear) and a soft material (TengoBlackPlus). By varying the internal pressure within each chamber, the actuator can elongate, compress, and bend in any radial direction. The bellow design folds and unfolds during actuation reducing the tensile stress in the material as compared to comparable straight-tube elastomeric design [28].

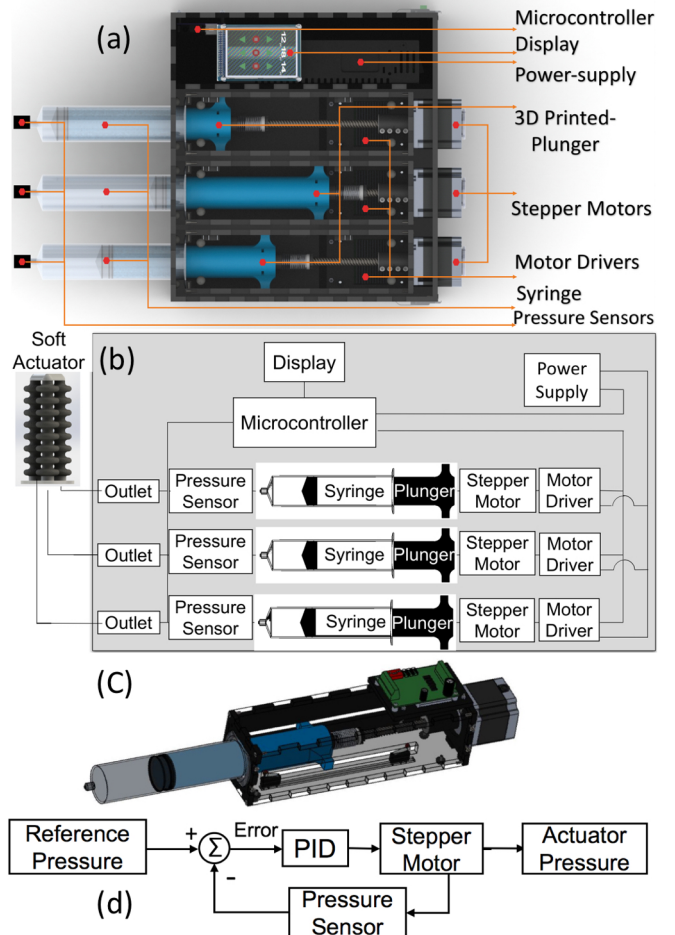


Fig. 2: Volumetric Control System Design: a) Rendered image of the system with main components annotated. b) Schematic drawing of the system illustrating the interconnections of the components. c) A single syringe pump module detached from the main system. d) Block diagram of the PID control loop implemented in each module

C. Contributions and Layout

In this paper, we describe a new volumetric control system for actuation of soft fluidic actuators and study the advantages of combining vacuum and pressure modes for 3D printed fluidic actuators. The contributions of this paper are

- The design of a low-cost system for volumetric pneumatic and hydraulic control of soft fluidic actuators.
- The description of an approach to employ the simultaneous vacuum and pressure (i.e. differential pressure) actuation for closed loop control of pneumatically actuated soft robots.
- Demonstration of improved performance of 3D printed soft fluidic actuators in terms of workspace, bend-angle, tip forces and robustness under combination of vacuum and pressure actuation.

In the next section (Section II) we present an overview of the design of the volumetric control system. The following section (Section III) discusses the experimental characterization of the 3D printed actuators with actuation using

differential pressure control. In section IV we describe the finite element model of the 3D printed actuator and present a simulation of the differential pressure actuation. Finally, Section V provides a conclusion and a brief discussion of future work.

II. VOLUMETRIC CONTROL SYSTEM DESIGN

For the purpose of actuating a large variety of soft fluidic actuators, (including the 3D printed soft actuators discussed above) we developed a modular volumetric control system (Fig.2). The system consists of interchangeable cylinder pump units that can be replaced if necessary or added depending on the application. Each unit is capable of inflating and deflating a chamber within a soft actuator by displacing fluidic volume.

The control system is composed of modular piston units. We chose to use commercially available plastic syringes to allow for adjustability in the displacement volume and type of actuation fluids while maintaining affordability and replaceability. We tested both 140cc and 200cc syringes, and used the latter for the experiments described in this paper. We replaced the plunger of each syringe with a 3D printed part with a center hole to accommodate a threaded rod. We used the rubber cap from the original syringe plunger on the 3D printed replacement to maintain the correct fit and prevent leaks. Each unit contains a stepper motor (Nema 23 CNC Stepper Motor 2.8A 178.5oz.in/1.26Nm), driven by a stepper motor driver (Uxcell TB6560 3A Single-Axis Stepper Motor Driver Board). Each motor rotates a threaded rod that drives a nut attached to the 3D printed plunger. As a result, rotational motion of the stepper motor is converted to linear motion of the plunger. The system is powered by a 360 W, 24 V power supply, controlled with a microcontroller (Arduino Mega 2560), and uses a display screen for visual interface. Each syringe outlet is mounted with a pressure sensor (SSCDANT150PGAA3 Honeywell Pressure Sensor) for pressure feedback. Table I lists the costs of components which form the volumetric control system.

TABLE I: Bill of Materials

Component	Quantity	cost per item	Total cost
200cc Plastic Syringe	3	\$17	\$51
Nema 23 Stepper Motor	3	\$26	\$78
Stepper Motor Driver	3	\$10	\$30
Threaded Rod 3'	1	\$8	\$8
Leadnut and Coupler	3	\$35	\$105
Power Supply	1	\$23	\$23
Microcontroller	1	\$35	\$35
Display	1	\$28	\$28
Pressure Sensor	3	\$41	\$123
Total			\$481

We implemented a closed-loop PID controller with actuator pressure feedback for error calculation. The block diagram of the control loop can be seen in (Fig. 2(d)).

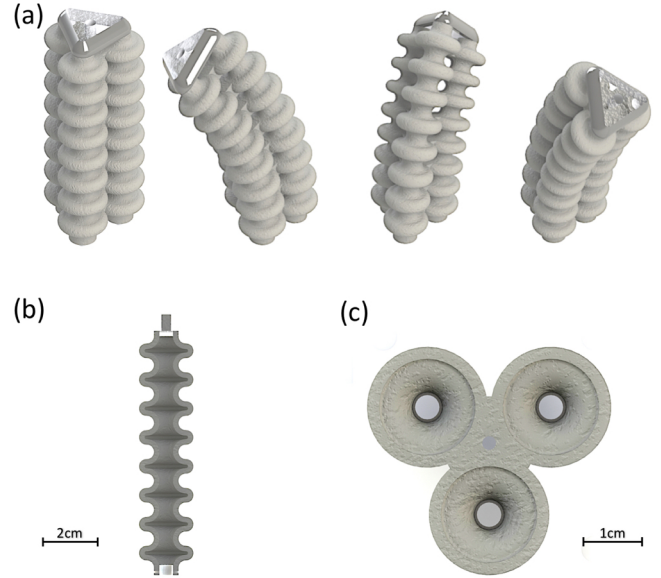


Fig. 3: 3D Printed Soft Actuator: a) Actuation of different chambers of the actuator. b) Radial plane cross section of a single chamber. c) Transverse plane cross-section of the actuator.

III. EXPERIMENTAL CHARACTERIZATION

We chose a set of experiments to evaluate performance metrics to compare the operation of the volumetric control system based on actuator capabilities. G. Agarwal et al. [29] presented a criterion for evaluation of new soft actuators. This criterion uses the performance requirements of force output and required displacement which are needed to complete an action to gauge actuator's behavior and to design durable and effective actuators. We compared the actuators performance between the three different actuation modes: inflation or positive pressure, deflation or negative pressure and the combination of both applied to separate chambers in a single actuator. For the rest of this paper we will refer to pressure values relative to atmospheric pressure with positive pressure for gauge pressure and negative pressure for vacuum.

A. Working Pressure Limits

To get an accurate comparison between the different actuation modes and to characterize the limits of safe operation in term of output angles and forces, we first determined the failure point in each mode. The failure point is the actuation state at which the stresses generated by the pressure of the working fluid inside the chambers, relative to the external atmospheric pressure caused a rupture in the actuator wall. In this experiment, we first tested for failure points by applying pressure only to a single chamber, starting from 0 kPa and increasing by increments of 1.72 kPa (.25 psi) every ten seconds until rupture was observed. A delay of ten seconds between each increment was necessary to allow for the viscoelastic material to relax completely. For the vacuum failure point, we repeated the same experiment except with

decreasing pressure, down to the maximum negative pressure achievable by the volumetric control system (-95 kPa gauge). To find the failure point for combinations of vacuum and pressures, we first applied a constant negative pressure -69 kPa gauge to a single chamber. This value was selected for practical reasons (Although the system is capable of applying up to -95 kPa for the tested actuator, the operation of vacuuming brings the plunger close to its movement limit and does not leave enough space for control adjustments.) After vacuum was applied to a single chamber, the two adjacent chambers were inflated in increments of 1.72 kPa every ten seconds until one of the two inflated actuated chambers was ruptured.

We used these experimental results to set the limit pressures (see Table II) to prevent actuator damage in subsequent experiments. When actuating using only positive pressure, the actuators failed at an average pressure of 105 kPa. Our testing show that at the highest vacuum our system is capable of producing (-95 kPa) the actuators did not show any sign of failure. For the differential test, the pressurized chambers failed at an average pressure of 64 kPa. Based on these results we set the global limit for the actuators working pressure to 60 kPa.

TABLE II: Working Pressure Limits

Actuation Mode	Pressure	Vacuum	Differential
Average Failure Point (kPa)	105	N/A	64
Standard Deviation	0.25	N/A	1.44

B. Blocked Force Comparison

Blocked force (the force applied by an actuator when the tip displacement is constrained to be zero) is a critical parameter for characterizing an actuators capabilities. To compare how the three different modes of pressurization affect the performance of this actuator, we used an experimental test setup (Fig. 4) [30]] that measures the force applied by the bending actuator. The test setup is made up of a single axis load cell (FX1901, Measurement Specialties) mounted to test vertical force, a microcontroller (Arduino Uno) used to collect data from the load cell, a stepper motor (NEMA 17, Adafruit), and a stepper driver (Easy Driver, Sparkfun) to align the actuator with the load cell. The actuator was mounted horizontally with the tip aligned with the load cell, to measure the perpendicular force applied by the tip of the actuator. We tested the actuator with a negative pressure of -95 kPa applied to a single chamber, a positive pressure of 60 kPa applied to a single chamber, and a combination of -69 kPa two chambers and 60 kPa in the third chamber (all oriented to apply a downward force at the tip). The experiment was repeated four times for each actuation mode and the data was recorded for each trial. A comparison of the blocked force results in (Fig. 4) shows that a tip output force in the radial direction using positive pressure produced 1.57 N on average (this is consistent with our previous measurements for this case which averages 1.5 N

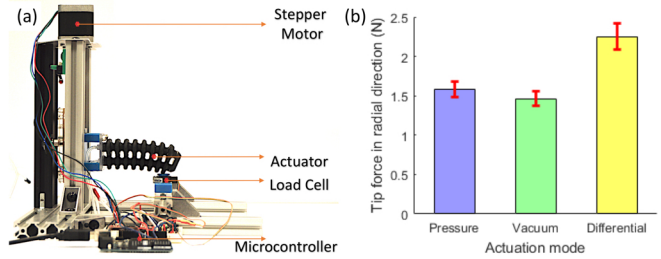


Fig. 4: a) Experimental test setup [27], [30] used to measure actuator force output. b) Tip force for different actuation modes (error bars represent standard deviation) Pressure test was performed at 60 kPa. Vacuum test was performed at -95 kPa gauge. Differential testing was performed with 60 kPa pressure and 69 kPa vacuum

[24]). The use of negative pressure similarly resulted in an average of 1.45 N force. However, the combination of vacuum and pressure resulted in an average of 2.25 N force, an improvement of 54% and 43% over actuation using only negative or positive pressure (respectively).

C. Actuator Workspace Comparison

The no-load displacement of the actuator was the second performance measure we used to compare the different actuation modes. We first measured the displacement in terms of bend angle of the module and secondly in terms of the elongation of the module. To evaluate the bend angle, we placed the actuator vertically and attached a needle to the actuator tip in the axial direction and measured the angle between the position of the needle before actuation and at the maximum deflection (Fig. 5). We repeated this experiment four times for each of the three actuation modes with pressure limits set by practical system limitations as discussed above (i.e. vacuum at -95 kPa, pressure at 60 kPa, and finally combination of negative pressure at -69 kPa with a positive pressure of 60 kPa for two actuators in vacuum and one in pressure and then for two actuators in pressure and one in vacuum).

The results of the differential test show an increase of 101% in the bend angle with respect to the positive pressure test and a 98% increase with respect to the negative pressure test. A polar plot of these results in (Fig. 5d) demonstrates the achievable bending angle in each spatial direction of the actuators for the different actuation modes. Note that only a third of the workspace is unique due to symmetry. For six of these points, the chambers are actuated at the positive and negative pressure limits listed in Table 1. For the six intermediate points, we determined the relative pressure values using the following relationship [14]

$$\tan(\theta) = \frac{(2P_1 - P_2 - P_3)}{(\sqrt{3}(P_2 - P_3))} \quad (1)$$

where P_i is the pressure in chamber i and θ is the azimuth angle of the bent actuator. This plot highlights the effective

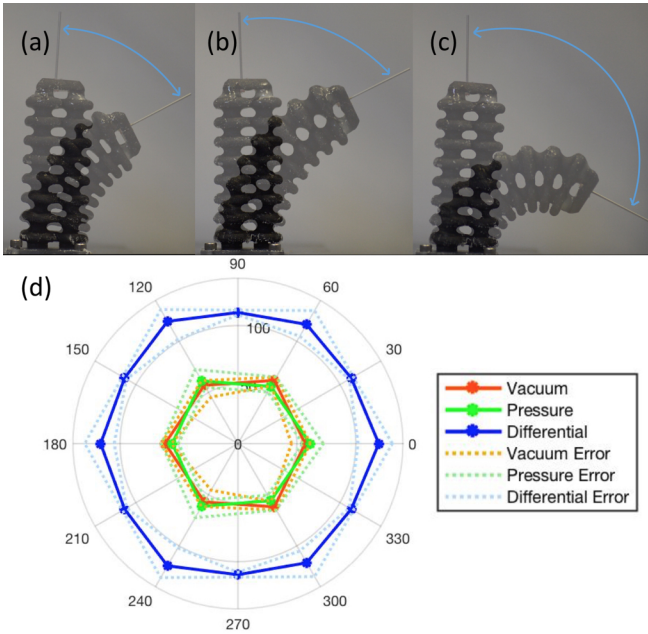


Fig. 5: Bending angle comparison measured from non-actuated position. a) Bending using only vacuum at -95 kPa. b) Bending using only pressure at 60 kPa. c) Differential pressure bending using combination of pressure at 60 kPa in two chambers and vacuum at -69 kPa in the third chamber. d) The average bending angle for each mode of actuation for 12 azimuth angles showing the increase in the actuator's work space

increase in the achievable workspace due to differential pressure. Three parameters: bend angle, azimuth angle, and elongation fully define the configuration of the actuator. Differential pressure control not only enables a higher bend angle but is also required to independently control these three degrees of freedom.

For the elongation test we evaluated the maximum linear displacement that can be achieved using differential pressure control for the soft actuator (Fig. 6). The maximum elongation with 60 kPa pressure in all three chambers was 15.6mm while the maximum shortening by applying -69 kPa in all three chambers was 21 mm. Overall the actuator underwent 37% axial deformation from minimum length to maximum length.

D. Operation of Ruptured Actuators with Negative Pressure Actuation

The most frequent failure mode for the 3D printed actuators is delamination of printed layers (Fig. 7a). Because 3D printing works by laying down successive layers of material, the strength of a part perpendicular to these layers is typically lower than the strength parallel to these layers. For this reason, we wanted to investigate an approach to recovering operation of ruptured actuators. For this experiment, we repeated the output force test and the bend angle comparison experiments for operation using only vacuum at -69 kPa and operation using only positive pressure at 60 kPa.

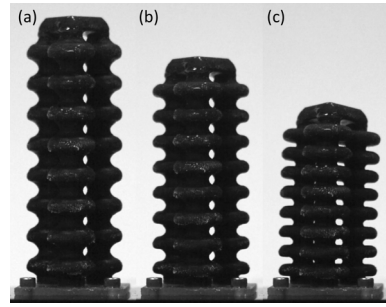


Fig. 6: Actuator linear displacement. a) Three chambers inflated to 69 kPa. b) Three chambers at 0 kPa. c) Three chambers at -60 kPa.

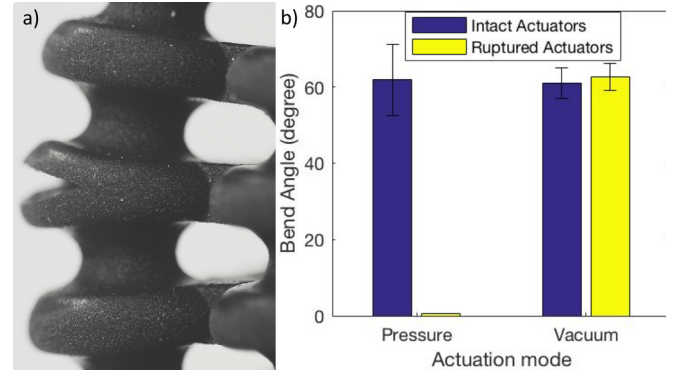


Fig. 7: a) A rupture created on the actuator due to delamination of the 3D printed layers. b) Actuator's bend angle comparison for different actuation with ruptured and intact actuators (error bars represent standard deviation)

The ruptured actuators which we tested with negative pressure did not show any sign of failure and their performance was at par with the undamaged actuators. On the other hand, the ruptured actuators we tested with positive pressure recorded 0 degrees bend angle and 0 N blocking force due to the air leakage through the rupture. (Fig. 7b) shows the actuators bend angle comparison for different actuation with ruptured and intact actuators.

E. Hand Writing Demonstration

To test the capabilities of the volumetric control system, we demonstrated the control of a soft actuator performing a continuous motion in the form of hand writing of text. We attached a laser pointer to the tip of the actuator in the axial direction to map the position of the tip to a planer sheet of paper (see Fig. 8 and supplementary video). A webcam was used to track the position of the laser pointer projected onto a sheet of paper. Closed loop control of the system relied on pressure feedback alone (i.e. without visual servoing).

To achieve an accurate continuous motion, we implemented a time delay between reference points along the actuator path to allow the actuator to complete its time dependent deformation caused by the viscoelastic 3D printed material used to print the actuators. Algorithm 1 summarizes the control algorithm used.

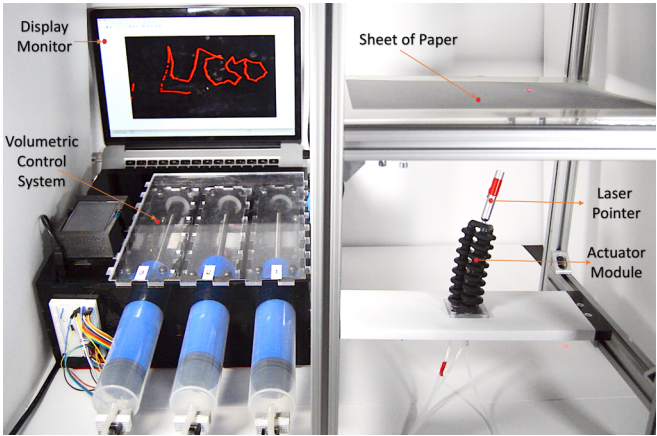


Fig. 8: Hand Writing Demonstration Setup. we manipulated the actuator with a laser pointer at the tip of it in the axial direction and a web-cam (not displayed) was used to track the laser light

Algorithm 1 Differential Pressure Actuation for Trajectory Control of Viscoelastic Actuator

Import set of reference pressures for each point in the trajectory of the actuator.

while actuator's path is not complete **do**

 Calculate the error of the pressure **if** not all three chambers are at their respective reference pressures.

then

 | Correct error of the pressures using PID controller

else

 | Wait ten seconds for the material to relax.

end

 Move to next reference point.

end

The letters produced following the above algorithm were displayed on a monitor (Fig. 8). The letters are connected since we did not control the on/off state of the laser. The precision of the system was demonstrated by repeating the same writing multiple times; the second loop exhibited a maximum deviation of 1.8 degrees from the first loop, and subsequent loops were almost indistinguishable from the previous iterations.

F. Suction Cup Manipulation Demonstration

A primary advantage of differential pressure control is the ability to extend and retract the actuator as demonstrated in the workspace comparison experiment. We devised a demonstration to exemplify a potential usage for this axial extension in soft robotics and the advantages of a control system with negative and positive pressure capabilities through a demonstration of grasping and manipulation of a fragile object (light bulb). We designed an actuator with a suction cup end effector that we actuated using a fourth syringe pump unit to apply a vacuum to the suction cup. The objective of the demonstration was for the actuator to approach the object, grasp it, complete a full rotation around the full workspace

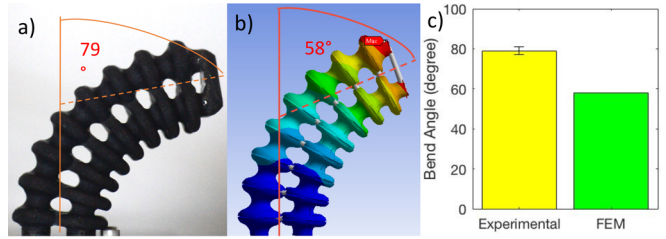


Fig. 9: Bending angle comparison for experimental and the finite element model with 60 kPa in a single chamber and -30 kPa in the other two chambers. a) Experimental results bending angle of 79 degrees. b) Simulation results bending angle of 58 degrees. c) Comparison of bend angle results (error bars represent standard deviation)

of the actuator and return the object to its initial position. The main challenge in the current demonstration were the carrying capacity and long-term manipulation caused by the limited sealing between the suction cup and the object (see Fig. 1a and supplementary video).

IV. FINITE ELEMENT ANALYSIS OF DIFFERENTIAL PRESSURE ACTUATION

The bellied actuator was simulated using the finite element method (FEM) software (ANSYS Inc. Mechanical) for actuation pressures up to 60 kPa (Fig. 9). The FEM model of the actuator is a surface model meshed with shell elements with the thickness of the actuator. The three actuation chambers are connected using beam elements. The experimental average bend angle was 79 degrees with a standard deviation of one degree. The FEM model simulation bending angle was much more conservative as it predicted a bending angle of 58 degrees.

The case with high vacuum pressure causes the bellows to collapse and come into contact with one another. As a consequence, the FEM analysis failed to converge for higher values of negative pressure due to the nonlinearities involved in the model. Alongside the material and structural non-linearities, the case with high vacuum pressure (i.e. less than -20KPa) also involves contact nonlinearities which inhibit convergence to a final solution using mixed (Normal Lagrange + Penalty) contact formulation. The FEM model uses beams to constrain the maximum diameter of the bellows together. In reality, the connecting members have some thickness which may affect the bending. Also, the material used for the bellow is viscoelastic. Due to the materials unknown viscoelastic properties, for the FEM model, we approximated the material as a hyperelastic with the Neo-Hookean material model. Hence, these two factors contribute to the discrepancies between the FEM model simulation and the experimental results. A further study of the FEM analysis of 3D printed bellied actuators driven by negative pressure is left to future work.

V. CONCLUSIONS

We demonstrated a volumetric control system for closed systems that utilizes differential pressure control for the

actuation of soft modules. Our results show an increase of 54% and 43% in blocking force using differential pressure as compared to negative and positive pressure respectively. The results from our displacement test define the reachable workspace of the actuator bending angle and axial displacement. The improved three-dimensional workspace achieved by differential pressure control could enable a wide range of highly maneuverable soft robots capable of complex movements and precise trajectory tracking as demonstrated in our hand writing and manipulation experiments. We also demonstrated the self-healing characteristic of vacuum actuation of ruptured actuators which failed under positive pressure but regained normal operation under negative pressure. This feature could be used to improve the robustness and lifetime of 3D printed soft robots. Further work has yet to be done to improve of the positioning control of the actuators with a faster response time. Long term operation still represents a major challenge for 3D printed soft actuators due to material permeability and low durability. Experimental testing for lengthy continuous actuation is yet to be explored. Nonetheless, we believe that this work demonstrates the promise of using low-cost, modular, volume control systems to actuate 3D printed soft robots, and that this approach will lead to promising new applications of this emerging technology.

REFERENCES

- [1] D. Rus and M. T. Tolley, "Design, fabrication and control of soft robots," *Nature*, vol. 521, no. 7553, pp. 467–475, 2015.
- [2] N. Lu and D.-H. Kim, "Flexible and stretchable electronics paving the way for soft robotics," *Soft Robotics*, vol. 1, no. 1, pp. 53–62, 2014.
- [3] R. K. Katzschmann, A. D. Marchese, and D. Rus, "Autonomous Object Manipulation Using a Soft Planar Grasping Manipulator," *Soft Robotics*, vol. 2, no. 4, pp. 155–164, 2015.
- [4] M. Calisti, M. Giorelli, G. Levy, B. Mazzolai, B. Hochner, C. Laschi, and P. Dario, "An octopus-bioinspired solution to movement and manipulation for soft robots," *Bioinspiration & biomimetics*, vol. 6, no. 3, p. 036002, 2011.
- [5] M. T. Tolley, R. F. Shepherd, B. Mosadegh, K. C. Galloway, M. Wehner, M. Karpelson, R. J. Wood, and G. M. Whitesides, "A resilient, untethered soft robot," *Soft Robotics*, vol. 1, no. 3, pp. 213–223, 2014.
- [6] D. Katz and O. Brock, "Manipulating articulated objects with interactive perception," in *2008 IEEE International Conference on Robotics and Automation*, pp. 272–277, May 2008.
- [7] R. V. Martinez, J. L. Branch, C. R. Fish, L. Jin, R. F. Shepherd, R. M. D. Nunes, Z. Suo, and G. M. Whitesides, "Robotic tentacles with three-dimensional mobility based on flexible elastomers," *Advanced Materials*, vol. 25, no. 2, pp. 205–212, 2013.
- [8] T. Ranzani, G. Gerboni, M. Cianchetti, and A. Menciassi, "A bioinspired soft manipulator for minimally invasive surgery," *Bioinspiration & Biomimetics*, vol. 10, no. 3, p. 35008, 2015.
- [9] H. Ren, X. Gu, and K. L. Tan, "Human-compliant body-attached soft robots towards automatic cooperative ultrasound imaging," in *Computer Supported Cooperative Work in Design (CSCWD), 2016 IEEE 20th International Conference on*, pp. 653–658, IEEE, 2016.
- [10] M. Manti, A. Pratesi, E. Falotico, M. Cianchetti, and C. Laschi, "Soft assistive robot for personal care of elderly people," in *2016 6th IEEE International Conference on Biomedical Robotics and Biomechatronics (BioRob)*, pp. 833–838, June 2016.
- [11] A. D. Marchese, R. K. Katzschmann, and D. Rus, "A Recipe for Soft Fluidic Elastomer Robots," *Soft Robotics*, vol. 2, no. 1, pp. 7–25, 2015.
- [12] S. Kim, E. Hawkes, K. Choy, M. Joldaz, J. Foley, and R. Wood, "Micro artificial muscle fiber using niti spring for soft robotics," in *Intelligent Robots and Systems, 2009. IROS 2009. IEEE/RSJ International Conference on*, pp. 2228–2234, IEEE, 2009.
- [13] Y. Bar-Cohen, *Electroactive polymer (EAP) actuators as artificial muscles: reality, potential, and challenges*, vol. 136. SPIE press, 2004.
- [14] K. Suzumori, S. Iikura, and H. Tanaka, "Applying a flexible microactuator to robotic mechanisms," *IEEE Control Systems*, vol. 12, pp. 21–27, Feb 1992.
- [15] M. Luo, W. Tao, F. Chen, T. K. Khuu, S. Ozel, and C. D. Onal, "Design improvements and dynamic characterization on fluidic elastomer actuators for a soft robotic snake," in *Technologies for Practical Robot Applications (TePRA), 2014 IEEE International Conference on*, pp. 1–6, IEEE, 2014.
- [16] P. Polygerinos, N. Correll, S. A. Morin, B. Mosadegh, C. D. Onal, K. Petersen, M. Cianchetti, M. T. Tolley, and R. F. Shepherd, "Soft robotics: Review of fluid-driven intrinsically soft devices; manufacturing, sensing, control, and applications in human-robot interaction," *Advanced Engineering Materials*, pp. e201700016–n/a. e201700016.
- [17] R. K. Katzschmann, A. D. Marchese, and D. Rus, "Hydraulic autonomous soft robotic fish for 3d swimming," in *Experimental Robotics*, pp. 405–420, Springer, 2016.
- [18] A. D. Marchese, K. Komorowski, C. D. Onal, and D. Rus, "Design and control of a soft and continuously deformable 2D robotic manipulation system," *Proceedings - IEEE International Conference on Robotics and Automation*, pp. 2189–2196, 2014.
- [19] B. Mosadegh, P. Polygerinos, C. Keplinger, S. Wennstedt, R. F. Shepherd, U. Gupta, J. Shim, K. Bertoldi, C. J. Walsh, and G. M. Whitesides, "Pneumatic networks for soft robotics that actuate rapidly," *Advanced Functional Materials*, vol. 24, no. 15, pp. 2163–2170, 2014.
- [20] H. Apparatus, "Phd 2000 syringe pump series user's manual," 2011.
- [21] H. Lipson, "Challenges and Opportunities for Design, Simulation, and Fabrication of Soft Robots," *Soft Robotics*, vol. 1, no. 1, pp. 21–27, 2013.
- [22] H. Yabu, "Fabrication of mesoscale polymer structures by self," *IEEE Spectrum*, vol. 89, p. 43, 1989.
- [23] R. F. Shepherd, F. Ilievski, W. Choi, S. A. Morin, A. A. Stokes, A. D. Mazzeo, X. Chen, M. Wang, and G. M. Whitesides, "Multigait soft robot," *Proceedings of the National Academy of Sciences*, vol. 108, no. 51, pp. 20400–20403, 2011.
- [24] A. Zolfagharian, A. Z. Kouzani, S. Y. Khoo, A. A. A. Moghadam, I. Gibson, and A. Kaynak, "Evolution of 3D printed soft actuators," *Sensors and Actuators, A: Physical*, vol. 250, no. October, pp. 258–272, 2016.
- [25] B. N. Peele, T. J. Wallin, H. Zhao, and R. F. Shepherd, "3d printing antagonistic systems of artificial muscle using projection stereolithography," *Bioinspiration & biomimetics*, vol. 10, no. 5, p. 055003, 2015.
- [26] J. Morrow, S. Hemleben, and Y. Menguc, "Directly fabricating soft robotic actuators with an open-source 3-d printer," *IEEE Robotics and Automation Letters*, vol. 2, pp. 277–281, Jan 2017.
- [27] D. Drotman, S. Jadhav, M. Karimi, and M. T. Tolley, "3d printed soft actuators for a legged robot capable of navigating unstructured terrain *," in *Robotics and Automation (ICRA), 2014 IEEE International Conference on*, p. in press, IEEE, 2017.
- [28] G. Udupa, P. Sreedharan, P. Sai Dinesh, and D. Kim, "Asymmetric bellow flexible pneumatic actuator for miniature robotic soft gripper," *Journal of Robotics*, vol. 2014, 2014.
- [29] G. Agarwal, N. Besuchet, B. Audergon, and J. Paik, "Stretchable materials for robust soft actuators towards assistive wearable devices," *Nature Publishing Group*, vol. 6, p. 34224, 2016.
- [30] D. D. P. deZonia and M. T. Tolley, "Low-cost open-source mechanical tester for soft robotics," *2016 Robotics: Science and Systems Conference, Robot Makers: The future of digital rapid design and fabrication of robots*, 2016.